ACS APPLIED NANO MATERIALS

Improved Anticorrosion Properties of Polyurethane Nanocomposites by $Ti_3C_2T_x$ MXene/Functionalized Carbon Nanotubes for Corrosion Protection Coatings

Ding Lou, Hang Chen, Jinyuan Liu, Danling Wang, Congzhou Wang, Bharat K. Jasthi,* Zhengtao Zhu, Hammad Younes,* and Haiping Hong*

Cite This: https://doi.org/10.1021/acsanm.3c02316

Read Online

ACCESS | Metrics & More | Article Recommendations | SI Supporting Information

ABSTRACT: The corrosion protection of MXene-based composite coatings is challenging due to the relatively low dispersion of MXene in organic coatings. In this work, waterborne polyurethane (WPU) composites containing hybrid nanoadditives of $Ti_3C_2T_x$ MXene and functionalized carbon nanotubes (CNTs) were fabricated. The thermal stability, surface hydrophobicity, surface roughness, and mechanical properties of the nanocomposites containing MXene or MXene/CNT hybrid additives were studied. Electrochemical methods, including electrochemical impedance spectroscopy (EIS) and potentiodynamic polarization scans, were utilized to evaluate the anticorrosion properties of the nanocomposite coatings when applied to copper substrates. The polyurethane sample with 0.95 wt % $Ti_3C_2T_x$ MXene and 0.05 wt % CNTs showed the lowest corrosion rate of 2.1×10^{-3} μm year^{-1}. Additionally, the EIS results revealed that the corrosion resistance of WPU/MXene coatings significantly increased by adding 0.05 wt % CNTs. The mechanism of the improved anticorrosion performance of the WPU/MXene/CNT composite coating is illustrated. Moreover, the importance of optimizing the concentration of the CNTs is discussed to obtain better corrosion protection. The polyurethane nanocomposite coatings reported in this work present great potential as corrosion protection coatings for metals and other surfaces.

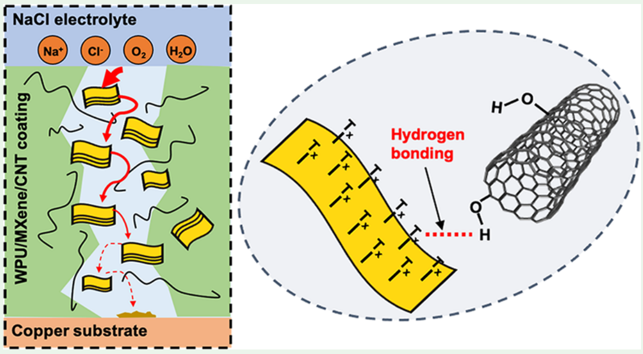

KEYWORDS: *$Ti_3C_2T_x$ MXene, functionalized carbon nanotubes, waterborne polyurethane, anticorrosion, nanocomposite coating*

1. INTRODUCTION

Global industries and communities have been suffering significant economic loss and environmental damage caused by the corrosion of metals and other surfaces. One of the most efficient and cost-effective ways of corrosion protection is to apply an organic coating on surfaces.[1,2] However, conventional organic coatings, such as polyurethane and epoxy, cannot provide sufficient corrosion protection as they tend to form cracks and micropores during the curing process. These structural defects allow corrosive molecules to easily penetrate the coating and attack the metal surface. Hence, researchers have developed nanocomposite coatings, of which nanomaterials were introduced to minimize the penetration of corrosive media.[3−5]

Over the past decades, two-dimensional (2D) nanomaterials have gained the most attention due to their large aspect ratio that can provide the maximum physical barrier effect.[6] Commonly utilized 2D materials for anticorrosion applications include but are not limited to graphene and graphene oxide,[7,8] hexagonal boron nitride,[9] molybdenum disulfide,[10] graphitic carbon nitride,[11] the MXene family,[12] etc. Recently, MXene as an emerging material has attracted increasing interest among the scientific community due to its optical, electrical, mechanical, and electrochemical properties.[13] MXene is a group of 2D layered materials with the general formula of $M_{n+1}X_nT_x$, where M is an early transition metal, X is a carbon or nitrogen atom, and T_x represents surface terminations. MXene is synthesized through selective etching of aluminum layers from its corresponding MAX phase.[14,15] Since the first synthesis of $Ti_3C_2T_x$ MXene in 2011,[16] MXene has been widely explored in various applications, such as supercapacitors, sodium/lithium-ion batteries, membrane capacitive deionization, etc.[17,18] Researchers have reported that MXene could enhance the anticorrosion properties of composite coatings, but the improvement was limited due to the natural

Received: May 23, 2023
Accepted: June 6, 2023

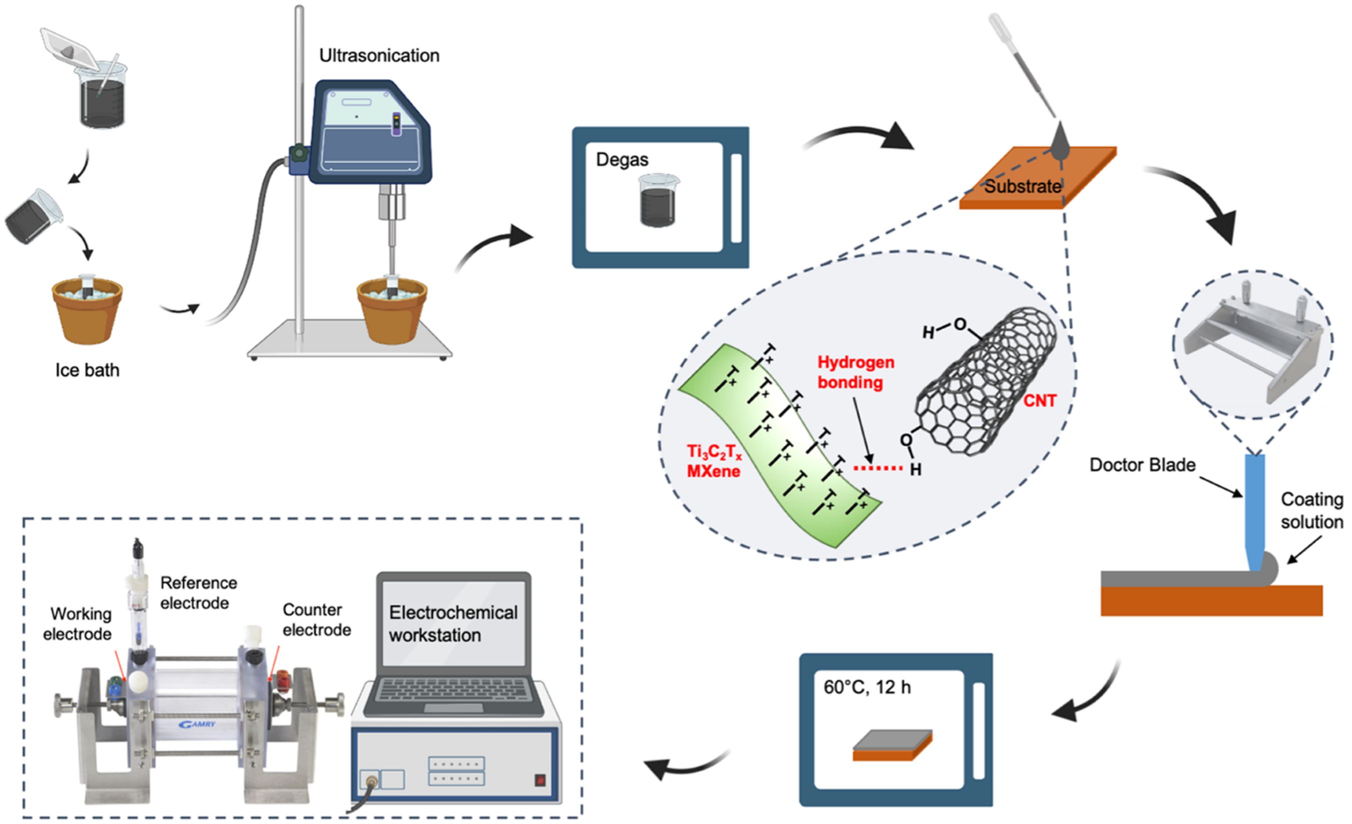

Figure 1. Schematic illustration of the nanocomposite fabrication. This figure is partially created on Biorender.com.

restacking of the MXene nanosheets. Therefore, it is critical to obtain good dispersion of MXene in order to achieve maximum corrosion inhibition.[15,19]

The improved dispersion of MXene in organic coatings can be achieved by covalent modification of MXene sheets, mostly amino-silane functionalization.[20,21] For example, Yan et al.[22] investigated the anticorrosion and antiwear properties of a waterborne epoxy (WEP) coating reinforced by amino-functionalized $Ti_3C_2T_x$ MXene. The introduced amino groups contributed to the uniform distribution of $Ti_3C_2T_x$ sheets as well as the enhanced adhesion of the coating to the metal substrate. Noncovalent modification is another approach to promoting the dispersion of MXene in polymer organic coatings. Si et al.[23] utilized three cationic surfactants to modify $Ti_3C_2T_x$ MXene and revealed that the interlayer spacing between MXene nanosheets was greatly increased. Lately, Zhao et al.[24] prepared air-stable $Ti_3C_2T_x$ MXene nanosheets modified by an imidazolium salt ionic liquid (IL) and evaluated the anticorrosion performance of the fabricated IL@MXene-WEP composite coating. It was demonstrated that the increased corrosion resistance was attributed to the excellent dispersion of IL-modified MXene nanosheets.

It has been a common strategy to combine 2D materials with other nanomaterials of different dimensions to form heterojunction structures.[25] Based on the unique combination of nanomaterials, the nanocomposites with binary nanoadditives have been extensively explored in various applications such as solid-state batteries, photocatalysis, electromagnetic interference shielding, etc.[26,27] In the field of corrosion inhibition, hybrid nanoadditives have been reported to show synergistic effects on improving the anticorrosion properties of composite coatings.[28] Hu et al.[29] studied the anticorrosion performance of epoxy coating reinforced by functionalized carbon nanotubes/graphene oxide (CNTs/GO) hybrid nanofillers, which showed enhanced corrosion protection compared to individual CNTs or GO. It was demonstrated that the CNTs acted as bridges to link the GO and further blocked the diffusion pathways of corrosive media. Zhou et al.[30] dispersed $Ti_3C_2T_x$ MXene with hexagonal boron nitride (h-BN) and measured the corrosion resistance of the $Ti_3C_2T_x$/h-BN/epoxy coating. Compared to epoxy coatings that contained only h-BN or MXene, the $Ti_3C_2T_x$/h-BN/epoxy coating showed the highest corrosion resistance and impedance modulus, which maintained 10^7 even after 21 days of immersion. In addition, the density functional theory simulation revealed that the boron and nitrogen vacancy defects significantly improved the adsorption stability between $Ti_3C_2T_x$ and h-BN. The enhanced anticorrosion performance of composite coatings loaded with 2D material-based nanohybrids is attributed to the reduced agglomeration as well as the increased effective aspect ratio of the 2D material, which further lengthens the diffusion paths of corrosive molecules.[31]

The CNT is a well-known one-dimensional (1D) nanomaterial that has been widely utilized in nanocomposite applications due to its superior electrical conductivity and ultrahigh mechanical strength.[32,33] While it remains controversial, the CNT is generally considered an effective nanoadditive for anticorrosive composite coatings, but the high electrical conductivity could accelerate metal corrosion once defects are formed.[34,35] In other words, the highly conductive CNTs would promote electron transfer and accelerate the electrochemical reactions at the composite-metal interface. Besides, unlike 2D materials, the 1D CNT does not have a highly effective surface area or diameter-to-

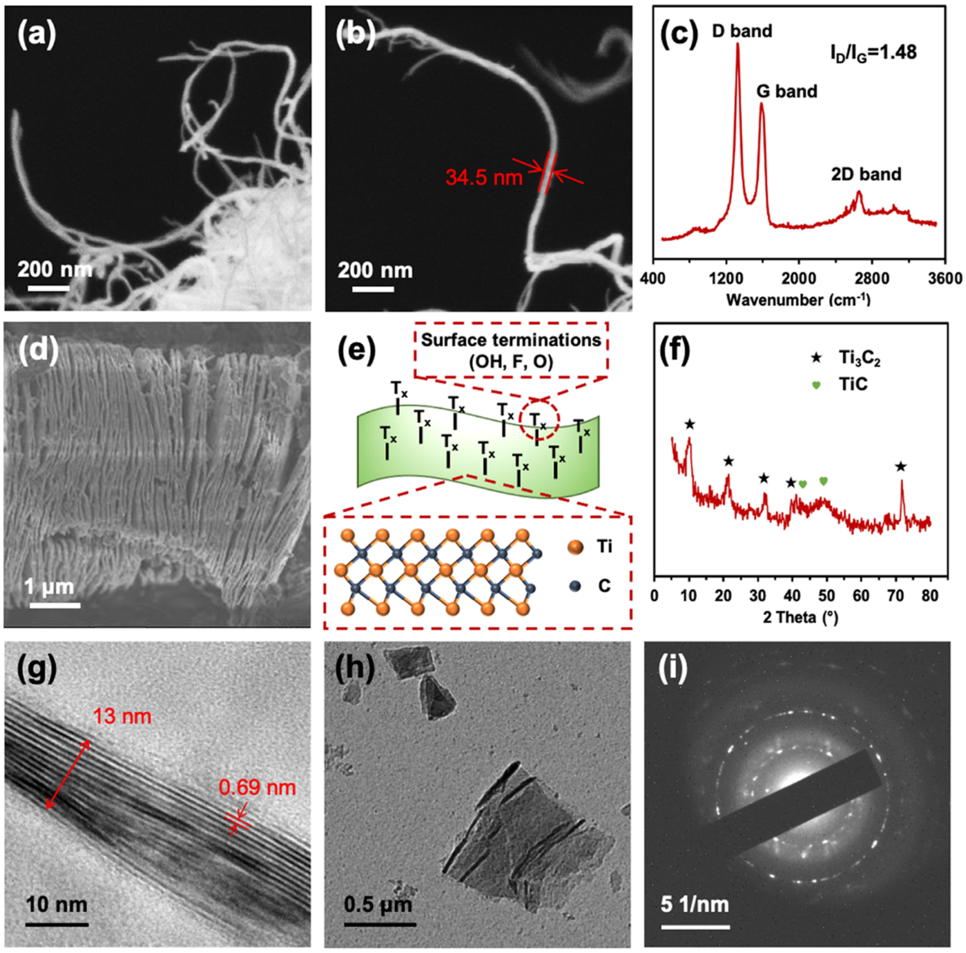

Figure 2. SEM images (a and b) and Raman spectrum (c) of as-received MWNT-OH. The SEM image (d), structure illustration (e), and XRD spectrum (f) of the synthesized $Ti_3C_2T_x$ MXene. (g–i) TEM characterizations of the synthesized $Ti_3C_2T_x$ MXene after sonication in absolute ethanol.

thickness ratio and therefore may not efficiently block the penetration of corrosive media. However, the combination of CNTs and 2D materials has been reported to provide enhanced properties as the CNTs improved the dispersion of 2D materials.[36,37] Wang et al.[38] prepared a waterborne polyurethane (WPU) coating with a hybrid of functionalized $Ti_3C_2T_x$ MXene and sodium dodecylbenzene sulfonate (SDBS)-modified CNTs. The fabricated composite coating effectively extended the penetration of corrosive molecules and provided sufficient corrosion protection after 120 days of immersion. However, the improvement in the impedance modulus of the hybrid composite coating was limited compared to $Ti_3C_2T_x$/WPU. To the best of the authors' knowledge, there are limited articles reporting the anticorrosion performance of composite coatings reinforced by MXene/CNT hybrid nanofillers. Hence, the facile and surfactant-free preparation of MXene/CNT-based composite coatings is worth investigating for the potential application of corrosion protection.

In this work, $Ti_3C_2T_x$ MXene and hydroxyl-functionalized multiwalled carbon nanotubes were dispersed in waterborne polyurethane. The surface terminations of MXene and the hydroxyl groups on CNTs enabled the formation of hydrogen bonding interactions, which significantly improved the dispersion of both nanofillers.[39] The nanocomposites were coated on copper substrates for anticorrosion studies through electrochemical methods. Additionally, the hydrophobicity, surface roughness, and mechanical properties of the nanocomposite samples were evaluated. The effect of using MXene/CNT hybrid nanoadditives on improving the properties of WPU was studied and the anticorrosion mechanism was illustrated.

2. EXPERIMENTAL SECTION

2.1. Materials. Waterborne polyurethane (WPU) was purchased from Menards. Hydroxyl-functionalized multiwalled carbon nanotubes (MWNT-OH, 20–40 nm diameter, 10–30 μm length, 95% purity) were purchased from Times Nano, China. $Ti_3C_2T_x$ MXene was synthesized through the selective etching of Al from the Ti_3AlC_2 MAX phase. The synthesis process was reported in previous work,[40] and the details of the synthesis are described in the Supporting Information.

2.2. Fabrication of Composite Coatings. $Ti_3C_2T_x$ MXene and MWNT-OH were added into WPU with desired concentrations. After stirring for 10 min, the coating solution was sonicated for 30 min in an ice bath to achieve uniform distribution. The coating solution was then degassed and applied on the copper substrates (25.4 mm × 25.4 mm × 3.2 mm) using a doctor blade. Before applying coating solutions, the copper substrates were polished to 600 grit, washed and air-blow dried, and finally cleaned with acetone. After curing at room temperature for 24 h, the coated samples were placed in a vacuum oven at 60 °C for 12 h. For comparison, neat WPU and the composite samples with only $Ti_3C_2T_x$ MXene were prepared. The fabrication process is illustrated in Figure 1. Table S1 (Supporting Information)

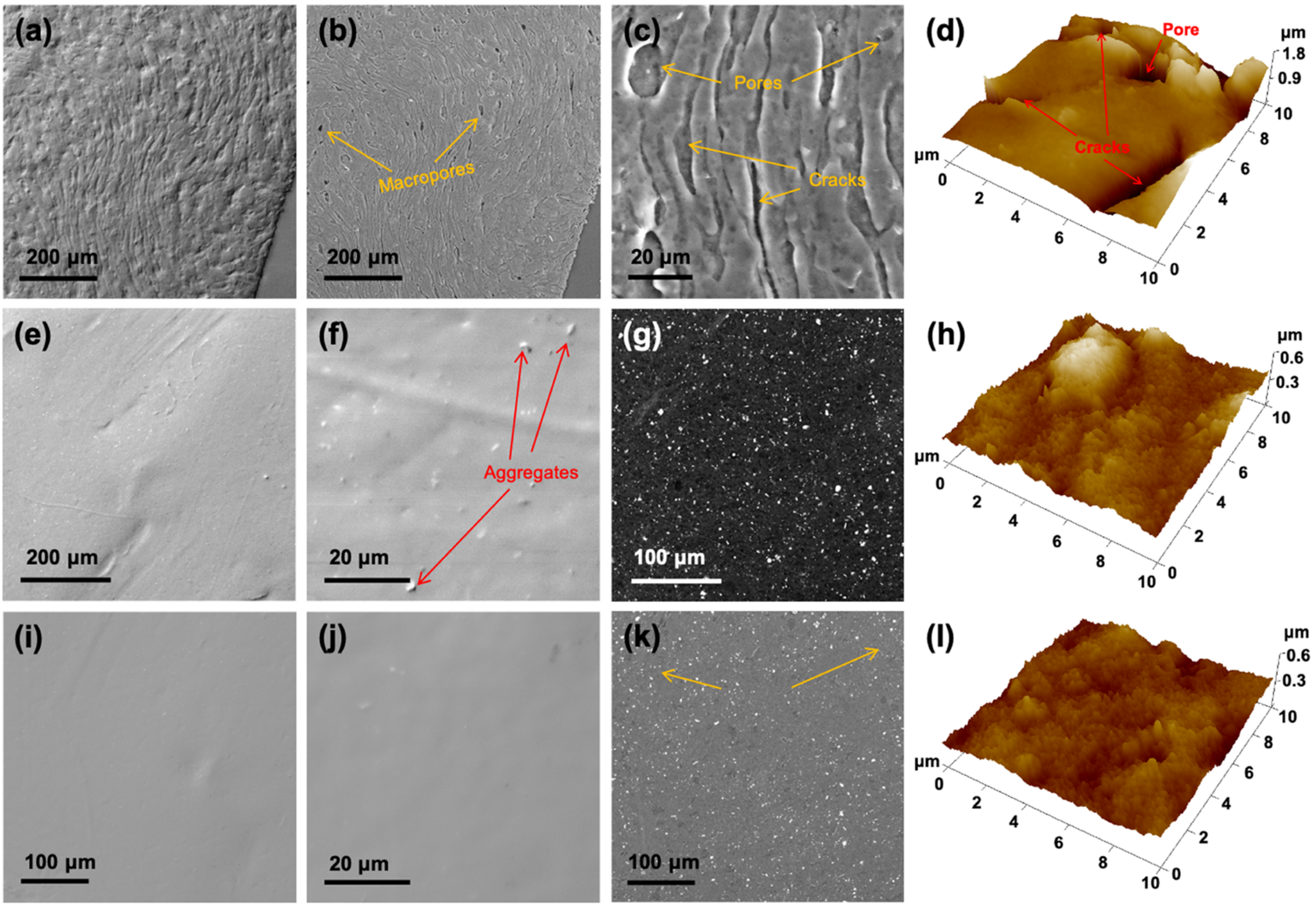

Figure 3. Backscattered electron images of neat WPU and the composite samples. Topographical (a), compositional (b and c), and 3D AFM (d) images of WPU; topographical (e and f), compositional (g), and 3D AFM (h) images of WPUMX1.0; and topographical (i and j), compositional (k), and 3D AFM (l) images of WPUCT0.05MX0.95.

lists the concentration details of the coating samples. The nanocomposite samples were labeled as "WPU," followed by the nanomaterial(s) and the concentration of the nanomaterial(s). For example, the WPU nanocomposite containing 0.05 wt % CNT and 0.95 wt % MXene was denoted as WPUCT0.05MX0.95.

2.3. Characterizations. $Ti_3C_2T_x$ MXene and MWNT-OH were characterized by a Helios 5 DualBeam scanning electron microscope (SEM), JEOL JEM 2100 LaB_6 transmission electron microscope (TEM), Foster+Freeman Foram Raman spectroscope, and Malvern Panalytical Empyrean X-ray diffraction spectroscope (XRD) with a cobalt source (λ = 0.1789 nm). The fabricated composite coatings were characterized by a scanning electron microscope, Thermo Scientific IS50 Fourier transform infrared (FT-IR) spectrometer, and SDT-Q600 thermogravimetric analysis (TGA) instrument. The surface roughness of the coatings was investigated using a Bruker BioScope Resolve atomic force microscope (AFM). The static water contact angles were measured to determine the hydrophobicity of the coatings. The sheet resistance of the composite samples was measured using a linear-array four-point setup connected with a Keithley multimeter. Nanoindentation was performed to measure the hardness of the composites using a Hysitron TI-980 Nanoindenter with a Berkovich tip. The maximum load was set to 1000 μN with a ramping rate of 100 $\mu N\ s^{-1}$. The hardness (H) and the reduced modulus (E_r) can be calculated by eqs 1 and 2

$$H = \frac{P_{max}}{A} \tag{1}$$

$$E_r = \frac{\sqrt{\pi}}{2}\frac{S_{max}}{\sqrt{A}} \tag{2}$$

where P_{max} is the maximum load, A is the projected contact area, and S_{max} is the slope of the unloading curve at maximum load. For a Berkovich tip, the contact area is calculated using eq 3, where h_p is the contact depth between the sample surface and the indenter.

$$A = 24.5{h_p}^2 \tag{3}$$

2.4. Electrochemical Measurements. The electrochemical measurements, including potentiodynamic polarization (PDP) scans and electrochemical impedance spectroscopy (EIS), were performed using a Gamry Instruments Reference 600+ Potentiostat/Galvanostat/ZRA connected to a Gamry three-electrode cell, of which the counter electrode is graphite and the reference electrode is Ag/AgCl in a 3 M KCl solution. The electrolyte solution was a 3.56 wt % NaCl solution. Both the PDP and EIS measurements were carried out after achieving a stable open circuit potential (OCP, 50 min in this work). PDP scans were performed at a voltage range of −1.0 to 1.0 V (vs OCP) with a scan rate of 1.0 mV s^{-1}. PDP curves were obtained by plotting the potential vs the logarithm of the current response. The corrosion current (i_{corr}) was calculated using the Stern−Geary equation (eq 4) and the corrosion rate (mm per year) was calculated using eq 5. The EIS measurements were carried out in a frequency range of 10^{-2} to 10^5 Hz with a signal amplitude interval of 10 mV.

$$i_{corr} = \frac{\beta_a\beta_c}{\beta_a + \beta_c} \times \frac{1}{2.303R_p} = \frac{B}{R_p} \tag{4}$$

where β_a and β_c are the anodic and cathodic Tafel constants, B is the Stern−Geary coefficient, and R_p is the polarization resistance which is calculated from the slope of the current versus voltage curve.

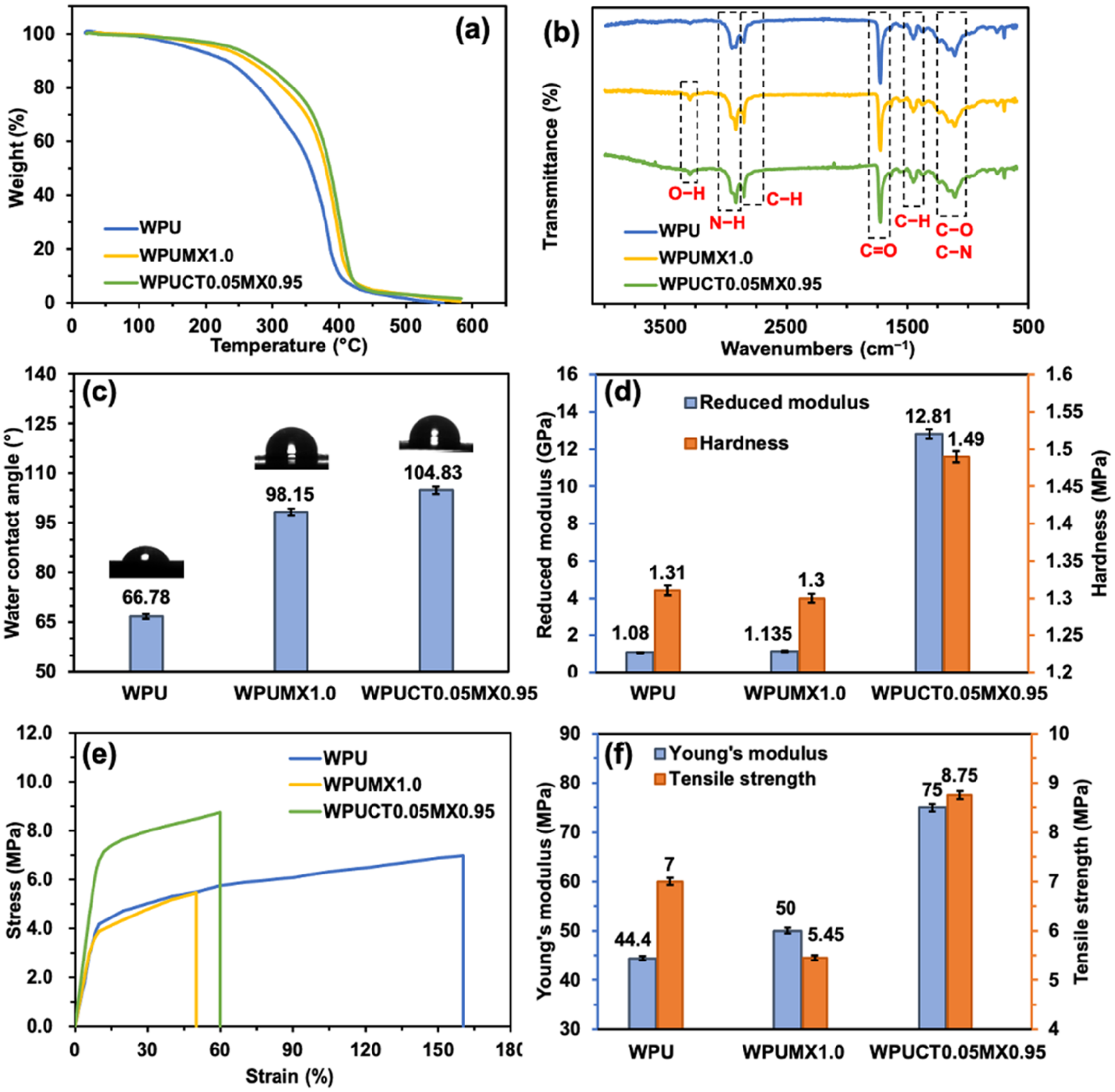

Figure 4. Characterizations of the fabricated nanocomposites. Thermogravimetric analysis (a), Fourier transform infrared spectra (b), the static water contact angle (c), the nanoindentation (d), the stress vs strain curves (e), and the calculated tensile strength, and Young's modulus (f) results of the neat WPU, WPUMX1.0, and WPUCT0.05MX0.95 nanocomposite samples.

$$\text{corrosion rate (mmpy)} = \frac{K \cdot \text{EW} \cdot i_{\text{corr}}}{D \cdot A} \tag{5}$$

where K is a constant (equals 3272 mm (A cm year)$^{-1}$), EW is the equivalent weight of the sample, D is the density of the sample, and A is the exposed area (2.85 cm^2) of the sample to the electrolyte solution.

3. RESULTS AND DISCUSSION

3.1. Morphologies and Structures. As-received MWNT-OH and the synthesized $Ti_3C_2T_x$ MXene were characterized using multiple techniques including SEM, TEM, Raman, and XRD. Figure 2a,b shows the SEM images of MWNT-OH showing a long, fibrous structure. The diameter of the carbon nanotubes ranges from 20 to 40 nm, matching the specification of the product. The average length of the nanotubes was hard to verify as they were entangled together due to the strong van der Waals force. Mechanical or chemical exfoliations are usually needed to disperse carbon nanotubes into a polymer composite or other systems. Figure 2c illustrates the Raman spectrum of MWNT-OH. Characteristic peaks were observed at 1324 and 1582 cm^{-1}, known as the D band and the G band, respectively. The ratio of the intensities of the D band to the G band (I_D/I_G) is 1.48, indicating a relatively high content of defects. The defects in the carbon nanotubes are often interpreted as sp^2 hybridized carbon (C═C) being converted to sp^3 carbon (C−C), which is mainly caused by the functionalization of the nanotubes through acid treatment.

The SEM image and the structure illustration of $Ti_3C_2T_x$ MXene are shown in Figure 2d,e. The SEM image reveals the multilayered 2D structure of the synthesized MXene. During the etching process, abundant surface terminations, including OH, F, and O, were introduced to the surface of the MXene sheets. Figure 2f shows the XRD characterization (cobalt source, λ = 0.1789 nm) of $Ti_3C_2T_x$ MXene. In the XRD spectrum, characteristic peaks are observed at (2θ) 10.1, 21.6, 31.8, 41.1, and 71.7° for Ti_3C_2.[41] The typical 2θ peak of Ti_3C_2 at 10.1°, assigned to the (002) plane,[42,43] corresponds to the d-spacing of 10.2 Å. The broad and weak interfering peaks at 40−50° represent the TiC residues. Figure 2g−i shows the TEM characterization of $Ti_3C_2T_x$ MXene after sufficient ultrasonication in absolute ethanol. The average thickness of multilayer MXene was measured to be 13 nm with an average distance of 0.69 nm between each layer. The lateral size of MXene ranges from 0.2 to 1.0 μm. The selected area electron diffraction (SAED) pattern of Figure 2i reveals hexagonal spots, demonstrating the hexagonal symmetry structure of $Ti_3C_2T_x$ MXene. It is seen that few-layer MXene is hard to obtain through ultrasonication or other mechanical methods as the MXene nanoflakes tend to restack. In this work, the improved dispersion is attributed to the hydrogen bonding between MXene and the functionalized CNTs, which also act as intercalation agents to prevent the restacking of the MXene nanoflakes.

The fabricated neat polyurethane and polyurethane-based nanocomposites were characterized by scanning electron microscopy using backscattered electron mode. The topographical and compositional images of WPU, WPUMX1.0, and WPUCT0.05MX0.95 are shown in Figure 3. It is seen that neat polyurethane has a rough surface with abundant macropores and cracks formed in the curing process. These pores and cracks allow corrosive molecules to easily penetrate the coating and attack the metal surface. While $Ti_3C_2T_x$ MXene flakes were added, the composite coating shows a much smoother surface with no obvious structural defects. The compositional image (g) shows the fairly homogeneous dispersion of MXene in polyurethane. However, aggregates are observed due to the restacking tendency of 2D MXene flakes. In comparison, the composite sample with both MXene and CNT exhibits a much more uniform surface with no apparent additive aggregates. Both the topographical and compositional images indicate that the dispersion of the MXene flakes may have been significantly improved by the addition of the hydroxyl-functionalized CNTs. The hydrogen interaction between the functional groups of MXene and CNT is considered key to improved dispersion. While homogeneously dispersed, the 1D CNTs act as the intercalation agents to further prevent the MXene flakes from restacking. Figures S1 and S2 (Supporting Information) show the cross-section SEM images of WPUMX1.0 and WPUCT0.05MX0.95 nanocomposites. In addition, energy-dispersive X-ray spectroscopy (EDS) was used to characterize the element distribution of the nanocomposite samples. The EDS results are shown in Figure S3 (Supporting Information). It is seen that the distribution of the Ti element in WPUMX1.0 is fairly good (Figure S3a) but is further improved in WPUCT0.05MX0.95 (Figure S3b).

The surface morphology of the composite samples was further characterized using AFM. Figure 3 shows the 3D AFM images of neat WPU (d), WPUMX1.0 (h), and WPUCT0.05MX0.95 (l). Cracks and macropores were observed for neat WPU, as expected. However, no obvious cracks or pores were observed from the composite samples that contain MXene or MXene/CNT additives. In addition, a microsized bump was observed in Figure 3h, which is likely attributable to the aggregation of $Ti_3C_2T_x$ MXene. The surface roughness of neat WPU was found to be 218 ± 8.4 nm. When MXene and CNTs were added, the composite samples showed much smoother surface topography than neat WPU. The surface roughness of WPUMX1.0 and WPUCT0.05MX0.95 was found to be 58.5 ± 1.7 and 45.1 ± 2.1 nm, respectively. The addition of $Ti_3C_2T_x$ MXene significantly reduced the surface roughness of the composite sample, and the surface became even smoother when CNTs were added as a secondary additive. More AFM images showing the surface morphology of WPU, WPUMX1.0, and WPUCT0.05MX0.95 are shown in Figure S4 (Supporting Information).

3.2. Composite Characterizations. Various techniques, including thermogravimetric analysis, Fourier transform infrared spectroscopy, static water contact angle, and nanoindentation were used to characterize the fabricated WPU, WPUMX1.0, and WPUCT0.05MX0.95 composite samples. Figure 4a shows the weight loss curves of the samples. Neat WPU has an extrapolated onset temperature (T_o) of 298 °C, while the T_o for WPUMX1.0 and WPUCT0.05MX0.95 are 346 and 352 °C, showing an increase of 16 and 18%, respectively. The first derivative plots of weight (%) vs temperature for the samples are shown in Figure S5 (Supporting Information). The first derivative peak temperature (T_p) for neat WPU is 387 °C, whereas the T_p for WPUMX1.0 and WPUCT0.05MX0.95 shows an increase of 1.6 and 5.2%, respectively. The results revealed an improvement in the thermal stability of the polyurethane composite with the addition of MXene or MXene/CNT. The FT-IR spectra of the samples are shown in Figure 4b. The broad peak at 1110 cm^{-1} represents the C−O and C−N stretching, and the small peak at 1453 cm^{-1} represents the C−H bending of the methyl group. The strong and sharp peak at 1726 cm^{-1} represents the C=O stretching of the urethane group. Several mild peaks interfere at 2800−3000 cm^{-1}, corresponding to the C−H stretching of alkane and the N−H stretching of the urethane group. It is observed that the N−H stretching of the composite samples (2918 cm^{-1}) is shifted by a few degrees compared to neat WPU (2921 cm^{-1}), indicating the influence of the hydrogen bonding that formed between the urethane groups and the functional groups of the nanoadditives. Additionally, an interfering peak at 2950 cm^{-1} is observed for WPUMX1.0 and WPUCT0.05MX0.95, representing the O−H stretching of the intramolecularly bonded hydroxyl groups. The small peak at 3298 cm^{-1} for WPUMX1.0 and WPUCT0.05MX0.95 indicates the existence of hydroxyl functional groups on MXene and CNT.

The hydrophobicity of the composite samples was evaluated by measuring the static water contact angle (WCA), as shown in Figure 4c. The WCA for neat WPU is 66.78°, demonstrating the hydrophilic nature of the material. When 1.0 wt % $Ti_3C_2T_x$ MXene is added, the fabricated nanocomposite sample shows hydrophobic nature and has a WCA of 98.15°. It is known that a higher WCA often leads to better corrosion protection of the coating as for its ability to repel water molecules more efficiently. The WPU with 0.95 wt % $Ti_3C_2T_x$ MXene and 0.05 wt % CNT shows a higher WCA of 104.83°. Figure 4d shows the hardness results of the composite samples obtained from the nanoindentation test. It is seen that the WPUMX1.0 sample has similar hardness and reduced modulus with neat WPU. However, the WPUCT0.05MX0.95 sample shows a hardness of 1.49 MPa, which is 14.6% higher compared to WPUMX1.0. The reduced modulus of WPUCT0.05MX0.95 is 12.81 GPa, which is a significant increase from that of WPUMX1.0.

A tensile test was performed to further evaluate the mechanical properties of the composite samples. A schematic illustration of the tensile test is shown in Figure S6 (Supporting Information). Figure 4e shows the stress−strain curves of the neat WPU, WPUMX1.0, and WPUCT0.05MX0.95 nanocomposite samples, of which the calculated tensile strength and Young's modulus are compared in Figure 4f. It is seen that the addition of 1.0 wt % MXene

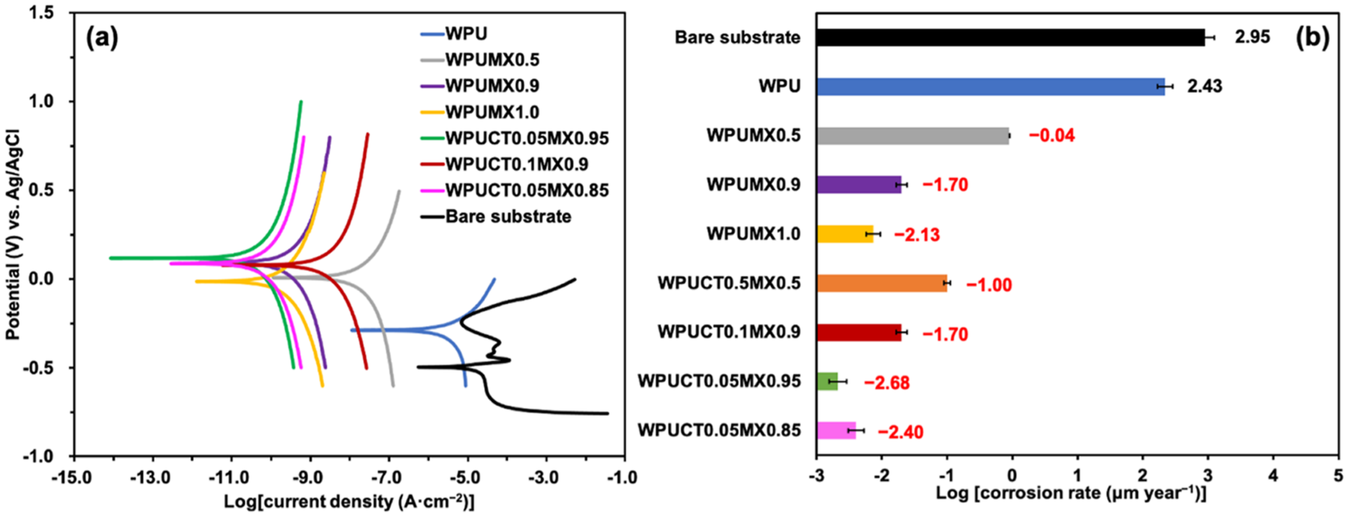

Figure 5. (a) Potentiodynamic polarization curves of the bare substrate and the specimens coated with neat WPU or WPU-based nanocomposites in 3.56 wt % NaCl and (b) corrosion rates of the bare substrate and the specimens coated with neat WPU or WPU-based nanocomposites extracted from PDP parameters.

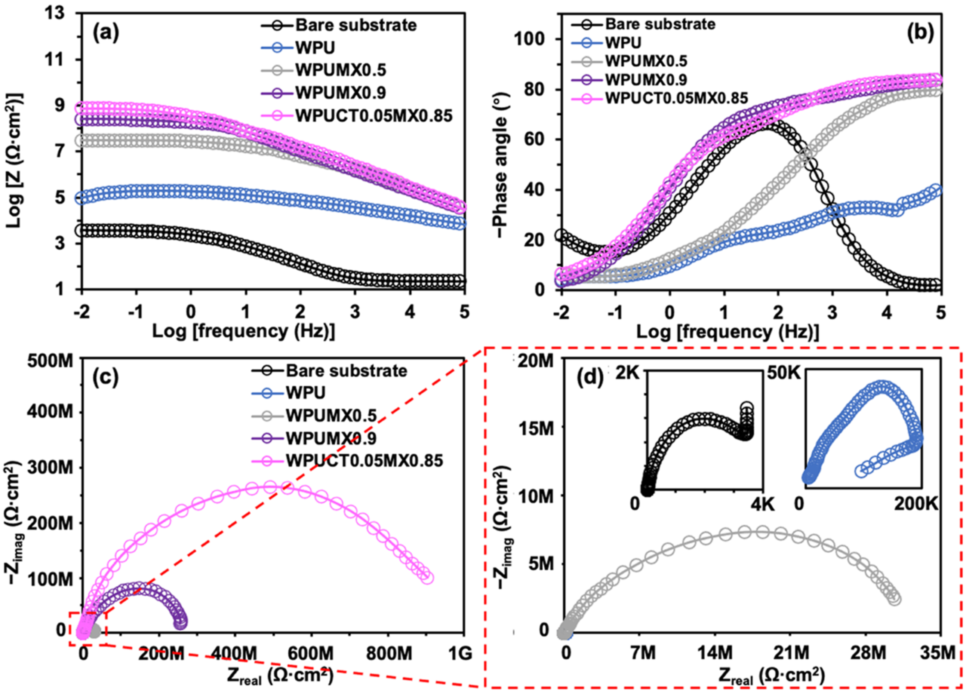

Figure 6. Bode plots (a and b) and Nyquist plots (c and d) of the bare substrate and the specimens coated with neat WPU or WPU-based nanocomposites in 3.56 wt % NaCl.

does not provide an obvious increase in tensile strength compared to neat WPU. On the contrary, the ultimate tensile strength of WPUMX1.0 is even lower than that of WPU. However, both the tensile strength and Young's modulus significantly increase when 0.05 wt % CNT was added. Compared to the polyurethane sample with only MXene (WPUMX1.0), WPUCT0.05MX0.95 shows a 50% increase in Young's modulus and a 60.6% increase in tensile strength. Both the nanoindentation results and the tensile test results reveal the positive effect of CNT on improving the mechanical properties of MXene nanocomposites. This improvement is mainly attributed to the high mechanical strength of the carbon nanotube itself as well as the improved dispersion of the additives that leads to stronger interactions between the polymer molecules and the nanoparticles.

3.3. Electrochemical Measurements. *3.3.1. Potentiodynamic Polarization Scan.* The anticorrosion properties of the composite coatings were investigated by potentiodynamic polarization scans in a 3.56 wt % NaCl solution. Figure 5a shows the PDP curves of the bare substrate and the coated samples. It is seen that all of the samples containing nanofillers resulted in smaller current densities and more positive corrosion potentials compared to pure polyurethane. Table S2 (Supporting Information) summarizes the PDP parameters of the bare substrate and coated samples. Figure 5b shows the corrosion rate comparison of the bare substrate and the coated samples. With the increase of $Ti_3C_2T_x$ MXene content, the

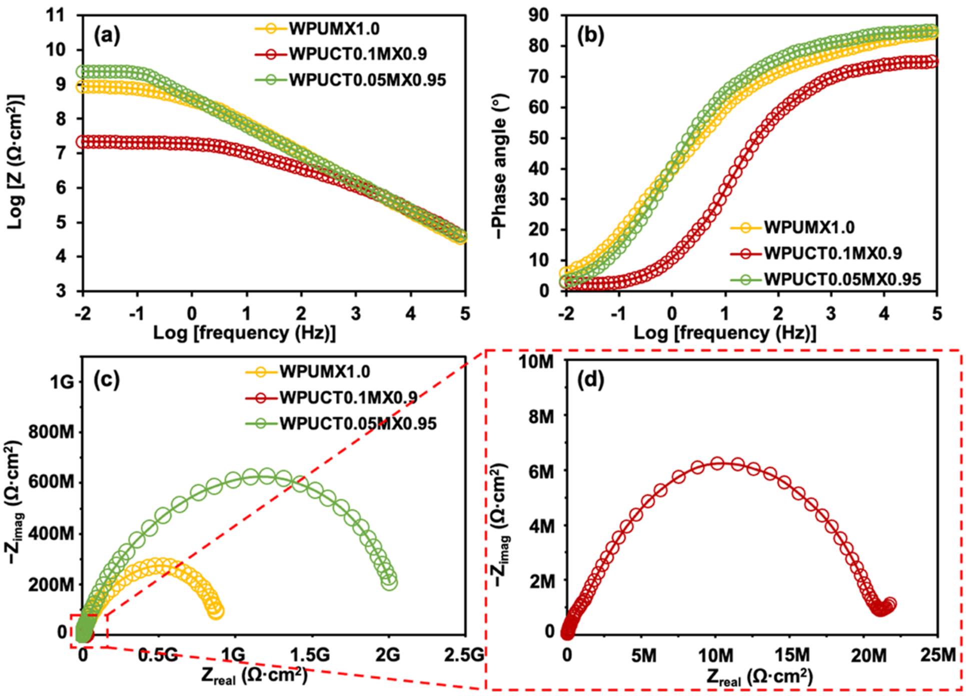

Figure 7. Bode plots (a and b) and Nyquist plots (c and d) of the specimens coated with WPUMX1.0, WPUCT0.1MX0.9, and WPUCT0.05MX0.95 in 3.56 wt % NaCl.

coated samples showed decreased corrosion current densities and corrosion rates, indicating the barrier effect of the MXene nanosheets. The polyurethane sample with 1.0 wt % MXene (WPUMX1.0) showed a significantly lowered corrosion rate of 7.4×10^{-3} μm year^{-1}. When 0.95 wt % MXene and 0.05 wt % MWNT-OH were added to WPU, and the lowest corrosion rate of 2.1×10^{-3} μm year^{-1} was obtained. Similarly, the corrosion rate of the sample containing 0.85 wt % MXene and 0.05 wt % MWNT-OH (WPUCT0.05MX0.85) was 4.0×10^{-3} μm year^{-1}, which was much lower than that of the sample containing 0.9 wt % MXene (WPUMX0.9). The results indicated that the anticorrosion properties of MXene polyurethane coatings were significantly enhanced by adding only 0.05 wt % of MWNT-OH. The reason is that the dispersion of the MXene nanosheets is improved by 1D carbon nanotubes through the hydrogen interactions between $Ti_3C_2T_x$ MXene and MWNT-OH. The improved dispersion of MXene nanosheets led to lengthened paths for the corrosive molecules, which consequently improved the corrosion resistance of the composite coatings. However, when a combination of 0.9 wt % MXene and 0.1 wt % MWNT-OH was added, the sample (WPUCT0.1MX0.9) showed a much higher corrosion rate. The reason might be that the MXene nanosheets and the high content of carbon nanotubes have built a well-connected network that enabled more efficient transport of electrons, which accelerated the corrosion reactions at the coating−substrate interface.

3.3.2. Electrochemical Impedance Spectroscopy. To further investigate the anticorrosion properties of the polyurethane samples containing MXene or MXene/CNT hybrid, electrochemical impedance spectroscopy was performed. The EIS results of the bare substrate and the coated samples are presented in Figures 6 and 7, and the equivalent electric circuit (EEC) models for the bare substrate and the coated samples are shown in Figure 8. Table S3 (Supporting Information) summarizes the EEC parameters by fitting the EIS plots to the EEC models. It is seen from the Bode plots that the impedance modulus of the WPU sample containing 1.0 wt % MXene (WPUMX1.0) is about four orders of magnitude higher than that of neat WPU, and the phase angles of the MXene-based samples reached about 80° at high frequency. The Nyquist plots illustrate that the semicircles of the MXene-based samples are significantly bigger than that of neat WPU. These results further support the results obtained from PDP scans, and it is concluded that the MXene nanofiller increased the corrosion resistance of the polyurethane coating. In addition, the impedance modulus of the sample containing 0.95 wt % MXene and 0.05 wt % MWNT-OH (WPUCT0.05MX0.95) at 0.01 Hz is higher than that of the sample containing 1.0 wt % MXene (WPUMX1.0). Similarly, the impedance modulus of the sample containing 0.85 wt % MXene and 0.05 wt % MWNT-OH (WPUCT0.05MX0.85) at 0.01 Hz is higher than that of the sample containing 0.9 wt % MXene. The EIS results further proved the improved dispersion of MXene nanosheets by the addition of 0.05 wt % MWNT-OH. It is worth noting that for sample WPU, the impedance in the Bode plot decreased and the Nyquist plot formed a loop at the low-frequency range. These unusual results indicate that there might be severe defects, especially holes, at the surface of the coating, which usually appear as inductance elements in the equivalent electrical circuit. This is because waterborne polyurethane tends to form cracks and holes when it cures. Therefore, more attention should be paid to the sample preparation process as the electrochemical system is so sensitive that every small issue will be magnified and reflected in the plots. However, they do not appear when nanomaterials are added, indicating that the nanoadditives help preserve the integrity of the composite coating during the curing process. Furthermore, the corrosion resistance of the coating sample is largely increased even with only 0.5 wt % MXene, indicating the excellent anticorrosion property of MXene.

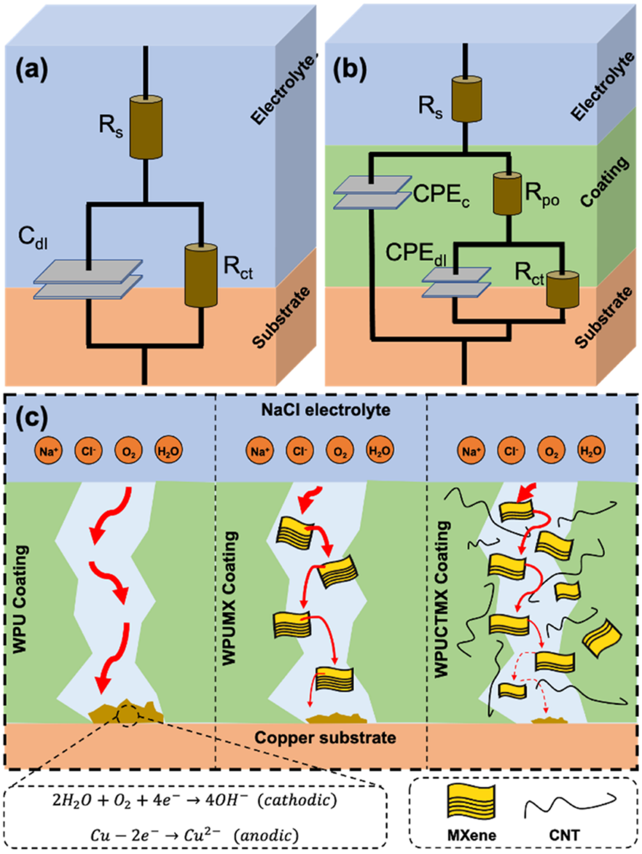

Figure 8. (a, b) Proposed equivalent electric circuit model for the bare substrate and the coated sample in the 3.56 wt % NaCl solution. R_s is the resistance of the solution, R_{ct} is the charge transfer resistance, R_{po} is the pore resistance, C_{dl}/CPE_{dl} is the double-layer capacitance, and CPE_c is the coating capacitance. CPE stands for the constant phase element, which is also known as an imperfect capacitor. (c) Mechanism sketches showing the anticorrosion behavior of the MXene or MXene/CNT hybrid additives.

3.4. Sheet Resistance.

To further understand the effect of the concentrations of CNTs on the corrosion protection performance, the sheet resistance of the composite samples was measured, and the results are summarized in Table 1. It is known that $Ti_3C_2T_x$ MXene and CNT are both electrically conductive materials. However, adding 1.0 wt % MXene did not make the WPU composite conductive due to the relatively low dispersion of the MXene nanosheets. When 0.05 wt % CNT was added, and the sample (WPUCT0.05MX0.95) remained nonconductive (out of range). With the increase of the CNT ratio, the sheet resistance of the composite samples decreased, owing to the conductive network formed between MXene and CNT. The sheet resistance reached as low as 23.8 KΩ when 0.5 wt % CNT and 0.5 wt % MXene were added into WPU. The results revealed that the sample WPUCT0.1MX0.9 was much more conductive than WPUCT0.05MX0.95, indicating the more efficient transport of electrons in WPUCT0.1MX0.9. Combined with the electrochemical measurements of these two samples, it was concluded that the improved conductivity of WPUCT0.1MX0.9 was mainly attributed to the decreased corrosion protection performance. Therefore, the concentration of CNTs needs to be strictly controlled to avoid the formation of efficient electron pathways.

Table 1. Measured Sheet Resistance Values of the Neat WPU and WPU-Based Nanocomposites

	sheet resistance (Ω sq^{-1})
WPU	>200 M (out of range)
WPUMX1.0	>200 M
WPUCT0.05MX0.95	>200 M
WPUCT0.075MX0.925	115 M
WPUCT0.1MX0.9	22 M
WPUCT0.2MX0.8	9.3 M
WPUCT0.5MX0.5	K

3.5. Mechanism.

The mechanism of the anticorrosion performance of the MXene or MXene/CNT coating on copper substrates is presented in Figure 8c. The mechanism sketches illustrate the easy penetration of the corrosive molecules through the cracks and pores that form in the neat polyurethane coating. When the corrosive molecules reach the surface of the copper substrate, corrosion is initiated, and the copper atoms start to lose electrons. Therefore, a higher charge transfer resistance often represents a lower corrosion rate. When MXene is dispersed in WPU, the corrosive pathways are significantly lengthened, resulting in much higher pore resistance and charge transfer resistance. However, the dispersion of MXene in the WPU system is limited due to its low compatibility and restacking tendency. The addition of CNTs improves the dispersion of MXene flakes because (i) hydrogen bonding forms between the hydroxyl groups of the CNTs and the surface terminations of MXene, and (ii) the CNTs act as intercalation agents to further separate the MXene flakes. Therefore, the penetration of the corrosive molecules is minimized using MXene/CNT hybrid nanoadditives. However, it is worth noting that an increase in the concentration of CNTs (0.1 wt %) leads to decreased resistance as the CNTs contribute to the interconnected percolation networks for electrons. The promoted electron transport leads to accelerated localized corrosion where electrolytes reach the surface. Therefore, this work reveals the efficient corrosion protection of the polyurethane composite coating by adding MXene/CNT hybrid nanomaterials. Additionally, it demonstrates the importance of optimizing the concentration of the CNTs to obtain better corrosion protection. Table S4 (Supporting Information) summarizes the corrosion rate and corrosion resistance of nanocomposites from this work and the literature.

4. CONCLUSIONS

Waterborne polyurethane coatings containing MXene or MXene/CNT hybrid nanoadditives were successfully fabricated. The thermal stability, surface hydrophobicity, surface roughness, and mechanical properties of the polyurethane-based composite coatings were studied. The anticorrosion properties of the composite coatings were evaluated using electrochemical methods. The main conclusions are summarized as follows:

(a) Compared to the WPU/MXene coating, the WPU/MXene composite containing 0.05 wt % CNTs exhibited higher thermal stability, a smoother and more hydrophobic surface, and reinforced mechanical properties.

(b) The WPU/MXene composite containing 0.05 wt % CNTs showed enhanced corrosion protection than WPU containing only MXene. It is mainly attributed to the improved dispersion of MXene by adding 0.05 wt % CNTs, which further lengthened the penetration pathways of the corrosive molecules.

(c) The hydrogen bonding formed between the hydroxyl groups of CNTs and the surface terminations of MXene is the main factor in achieving better dispersion of MXene flakes. In addition, the CNTs acted as intercalation agents and prevented the restacking of the MXene nanosheets.

(d) The electrochemical and sheet resistance measurements revealed the importance of optimizing the concentration of CNTs to obtain better corrosion protection. An increase in the concentration of CNTs (from 0.05 to 0.1 wt % or higher) would lead to accelerated corrosion reactions due to the interconnected networks for electron transport.

The polyurethane nanocomposite coatings reported in this work present great potential as corrosion protection coatings for metals and other surfaces.

■ ASSOCIATED CONTENT

SI Supporting Information

The Supporting Information is available free of charge at https://pubs.acs.org/doi/10.1021/acsanm.3c02316.

Synthesis of $Ti_3C_2T_x$ MXene; composition details of nanocomposites; SEM images of a cross-section of nanocomposites; EDS analysis of nanocomposites; AFM images of nanocomposites; TGA analysis of nanocomposites; tensile test scheme; electrochemical characterization results; and corrosion performance of nanocomposites (PDF)

■ AUTHOR INFORMATION

Corresponding Authors

Bharat K. Jasthi − *Department of Materials and Metallurgical Engineering, South Dakota School of Mines and Technology, Rapid City, South Dakota 57701, United States;* Email: Bharat.Jasthi@sdsmt.edu

Hammad Younes − *Department of Electrical Engineering, South Dakota School of Mines and Technology, Rapid City, South Dakota 57701, United States;* Email: hasy193@yahoo.com

Haiping Hong − *Department of Electrical Engineering, South Dakota School of Mines and Technology, Rapid City, South Dakota 57701, United States;* orcid.org/0000-0003-2190-3332; Email: haipinghong0619@gmail.com

Authors

Ding Lou − *Nanoscience and Nanoengineering, South Dakota School of Mines and Technology, Rapid City, South Dakota 57701, United States;* orcid.org/0000-0001-9117-5807

Hang Chen − *Institute for Electronics and Nanotechnology, Georgia Institute of Technology, Atlanta, Georgia 30332, United States*

Jinyuan Liu − *Nanoscience and Nanoengineering, South Dakota School of Mines and Technology, Rapid City, South Dakota 57701, United States*

Danling Wang − *Department of Electrical Engineering, North Dakota State University, Fargo, North Dakota 58102, United States;* orcid.org/0000-0003-0119-441X

Congzhou Wang − *Nanoscience and Nanoengineering, South Dakota School of Mines and Technology, Rapid City, South Dakota 57701, United States;* orcid.org/0000-0001-6132-447X

Zhengtao Zhu − *Department of Chemistry, Biology, and Health Sciences, South Dakota School of Mines and Technology, Rapid City, South Dakota 57701, United States;* orcid.org/0000-0002-9311-2110

Complete contact information is available at: https://pubs.acs.org/10.1021/acsanm.3c02316

Notes

The authors declare no competing financial interest.

■ ACKNOWLEDGMENTS

The authors would like to acknowledge the financial support provided through the Army Research Lab (Cooperative agreement W911NF 15-2-0034-S) and the National Science Foundation (RII Track-1#1849206 and RII Track-2 FEC#1920954). The authors would like to thank George Hong for proofreading the final edition of the manuscript.

■ REFERENCES

(1) Peng, T.; Xiao, R.; Rong, Z.; Liu, H.; Hu, Q.; Wang, S.; Li, X.; Zhang, J. Polymer Nanocomposite-based Coatings for Corrosion Protection. *Chem. - Asian J.* **2020**, *15*, 3915−3941.

(2) Cui, G.; Bi, Z.; Zhang, R.; Liu, J.; Yu, X.; Li, Z. A comprehensive review on graphene-based anti-corrosive coatings. *Chem. Eng. J.* **2019**, *373*, 104−121.

(3) Deyab, M. A. Anticorrosion properties of nanocomposites coatings: A critical review. *J. Mol. Liq.* **2020**, *313*, No. 113533.

(4) Ding, R.; Li, W.; Wang, X.; Gui, T.; Li, B.; Han, P.; Tian, H.; Liu, A.; Wang, X.; Liu, X.; Gao, X.; Wang, W.; Song, L. A brief review of corrosion protective films and coatings based on graphene and graphene oxide. *J. Alloys Compd.* **2018**, *764*, 1039−1055.

(5) Mu, J.; Gao, F.; Cui, G.; Wang, S.; Tang, S.; Li, Z. A comprehensive review of anticorrosive graphene-composite coatings. *Prog. Org. Coat.* **2021**, *157*, No. 106321.

(6) Shen, X.; Zheng, Q.; Kim, J.-K. Rational design of two-dimensional nanofillers for polymer nanocomposites toward multifunctional applications. *Prog. Mater. Sci.* **2021**, *115*, No. 100708.

(7) Li, J.; Cui, J.; Yang, J.; Li, Y.; Qiu, H.; Yang, J. Reinforcement of graphene and its derivatives on the anticorrosive properties of waterborne polyurethane coatings. *Compos. Sci. Technol.* **2016**, *129*, 30−37.

(8) Tong, Y.; Bohm, S.; Song, M. The capability of graphene on improving the electrical conductivity and anti-corrosion properties of Polyurethane coatings. *Appl. Surf. Sci.* **2017**, *424*, 72−81.

(9) Chilkoor, G.; Jawaharraj, K.; Vemuri, B.; Kutana, A.; Tripathi, M.; Kota, D.; Arif, T.; Filleter, T.; Dalton, A. B.; Yakobson, B. I.; Meyyappan, M.; Rahman, M. M.; Ajayan, P. M.; Gadhamshetty, V. Hexagonal Boron Nitride for Sulfur Corrosion Inhibition. *ACS Nano* **2020**, *14*, 14809−14819.

(10) Xia, Z.; Liu, G.; Dong, Y.; Zhang, Y. Anticorrosive epoxy coatings based on polydopamine modified molybdenum disulfide. *Prog. Org. Coat.* **2019**, *133*, 154−160.

(11) Pourhashem, S.; Duan, J.; Guan, F.; Wang, N.; Gao, Y.; Hou, B. New effects of TiO2 nanotube/g-C3N4 hybrids on the corrosion protection performance of epoxy coatings. *J. Mol. Liq.* **2020**, *317*, No. 114214.

(12) Yan, H.; Li, W.; Li, H.; Fan, X.; Zhu, M. Ti3C2 MXene nanosheets toward high-performance corrosion inhibitor for epoxy coating. *Prog. Org. Coat.* **2019**, *135*, 156−167.

(13) Carey, M.; Barsoum, M. W. MXene polymer nanocomposites: a review. *Mater. Today Adv.* **2021**, *9*, No. 100120.

(14) Gogotsi, Y.; Anasori, B. The Rise of MXenes. *ACS Nano* **2019**, *13*, 8491−8494.

(15) Gao, L.; Li, C.; Huang, W.; Mei, S.; Lin, H.; Ou, Q.; Zhang, Y.; Guo, J.; Zhang, F.; Xu, S.; Zhang, H. MXene/Polymer Membranes: Synthesis, Properties, and Emerging Applications. *Chem. Mater.* **2020**, *32*, 1703−1747.

(16) Naguib, M.; Kurtoglu, M.; Presser, V.; Lu, J.; Niu, J.; Heon, M.; Hultman, L.; Gogotsi, Y.; Barsoum, M. W. Two-dimensional nanocrystals produced by exfoliation of Ti3 AlC2. *Adv. Mater.* **2011**, *23*, 4248−4253.

(17) Zhang, L.; Yang, G.; Chen, Z.; Liu, D.; Wang, J.; Qian, Y.; Chen, C.; Liu, Y.; Wang, L.; Razal, J.; Lei, W. MXene coupled with molybdenum dioxide nanoparticles as 2D-0D pseudocapacitive electrode for high performance flexible asymmetric micro-supercapacitors. *J. Materiomics* **2020**, *6*, 138−144.

(18) Luo, J.; Gao, S.; Luo, H.; Wang, L.; Huang, X.; Guo, Z.; Lai, X.; Lin, L.; Li, R. K. Y.; Gao, J. Superhydrophobic and breathable smart MXene-based textile for multifunctional wearable sensing electronics. *Chem. Eng. J.* **2021**, *406*, No. 126898.

(19) Li, S.; Huang, H.; Chen, F.; He, X.; Ma, Y.; Zhang, L.; Sheng, X.; Chen, Y.; Shchukina, E.; Shchukin, D. Reinforced anticorrosion performance of waterborne epoxy coating with eco-friendly L-cysteine modified $Ti_3C_2T_x$ MXene nanosheets. *Prog. Org. Coat.* **2021**, *161*, No. 106478.

(20) Zhang, F.; Liu, W.; Wang, S.; Liu, C.; Shi, H.; Liang, L.; Pi, K. Surface functionalization of $Ti_3C_2T_x$ and its application in aqueous polymer nanocomposites for reinforcing corrosion protection. *Composites, Part B* **2021**, *217*, No. 108900.

(21) He, D.; Cai, M.; Yan, H.; Lin, Q.; Fan, X.; Zhang, L.; Zhu, M. Tribological properties of $Ti_3C_2T_x$ MXene reinforced interpenetrating polymers network coating. *Tribol. Int.* **2021**, *163*, No. 107196.

(22) Yan, H.; Cai, M.; Li, W.; Fan, X.; Zhu, M. Amino-functionalized Ti3C2T with anti-corrosive/wear function for waterborne epoxy coating. *J. Mater. Sci. Technol.* **2020**, *54*, 144−159.

(23) Si, J. Y.; Tawiah, B.; Sun, W. L.; Lin, B.; Wang, C.; Yuen, A. C. Y.; Yu, B.; Li, A.; Yang, W.; Lu, H. D.; Chan, Q. N.; Yeoh, G. H. Functionalization of MXene Nanosheets for Polystyrene towards High Thermal Stability and Flame Retardant Properties. *Polymers* **2019**, *11*, 976.

(24) Zhao, H.; Ding, J.; Zhou, M.; Yu, H. Air-Stable Titanium Carbide MXene Nanosheets for Corrosion Protection. *ACS Appl, Nano Mater.* **2021**, *4*, 3075−3086.

(25) Ding, J.; Zhao, H.; Yu, H. Structure and performance insights in carbon dots-functionalized MXene-epoxy ultrathin anticorrosion coatings. *Chem. Eng. J.* **2022**, *430*, No. 132838.

(26) Huang, H.; Sheng, X.; Tian, Y.; Zhang, L.; Chen, Y.; Zhang, X. Two-Dimensional Nanomaterials for Anticorrosive Polymeric Coatings: A Review. *Ind. Eng. Chem. Res.* **2020**, *59*, 15424−15446.

(27) Li, Y.; Zhou, B.; Shen, Y.; He, C.; Wang, B.; Liu, C.; Feng, Y.; Shen, C. Scalable manufacturing of flexible, durable $Ti_3C_2T_x$ MXene/Polyvinylidene fluoride film for multifunctional electromagnetic interference shielding and electro/photo-thermal conversion applications. *Composites, Part B* **2021**, *217*, No. 108902.

(28) Li, Q.; Liu, H.; Zhang, S.; Zhang, D.; Liu, X.; He, Y.; Mi, L.; Zhang, J.; Liu, C.; Shen, C.; Guo, Z. Superhydrophobic Electrically Conductive Paper for Ultrasensitive Strain Sensor with Excellent Anticorrosion and Self-Cleaning Property. *ACS Appl. Mater. Interfaces* **2019**, *11*, 21904−21914.

(29) Hu, H.; He, Y.; Long, Z.; Zhan, Y. Synergistic effect of functional carbon nanotubes and graphene oxide on the anticorrosion performance of epoxy coating. *Polym. Adv. Technol.* **2017**, *28*, 754−762.

(30) Zhou, M.; Zhao, C.; Liu, P.; Yu, H. Adsorption behavior of $Ti_3C_2T_x$ with h-BN nanosheet and their application in waterborne epoxy anti-corrosion coating. *Appl. Surf. Sci.* **2022**, *586*, No. 152778.

(31) Shen, L.; Zhao, W.; Wang, K.; Xu, J. GO-Ti3C2 two-dimensional heterojunction nanomaterial for anticorrosion enhancement of epoxy zinc-rich coatings. *J. Hazard. Mater.* **2021**, *417*, No. 126048.

(32) Li, Y.; Huang, X.; Zeng, L.; Li, R.; Tian, H.; Fu, X.; Wang, Y.; Zhong, W.-H. A review of the electrical and mechanical properties of carbon nanofiller-reinforced polymer composites. *J. Mater. Sci.* **2019**, *54*, 1036−1076.

(33) Li, Y.; Wang, Q.; Wang, S. A review on enhancement of mechanical and tribological properties of polymer composites reinforced by carbon nanotubes and graphene sheet: Molecular dynamics simulations. *Composites, Part B* **2019**, *160*, 348−361.

(34) Cui, C.; Lim, A. T. O.; Huang, J. A cautionary note on graphene anti-corrosion coatings. *Nat. Nanotechnol.* **2017**, *12*, 834−835.

(35) Elmi, F.; Valipour, E.; Ghasemi, S. Synthesis of anticorrosion nanohybrid films based on bioinspired dopamine, L-cys/CNT@PDA through self-assembly on 304 stainless steel in 3.5% NaCl. *Bioelectrochemistry* **2019**, *126*, 79−85.

(36) Qian, Y.; Zhong, J.; Ou, J. Superdurable fiber-reinforced composite enabled by synergistic bridging effects of MXene and carbon nanotubes. *Carbon* **2022**, *190*, 104−114.

(37) Zong, Z.; Ren, P.; Guo, Z.; Wang, J.; Hu, J.; Chen, Z.; Jin, Y.; Wang, F.; Ren, F. Synergistic effect of 2D TiC and 1D CNT towards absorption-dominant high-performance electromagnetic interference shielding in 3D macroporous carbon aerogel. *Carbon* **2022**, *197*, 40−51.

(38) Wang, Y.; Chang, W.; Wang, Z.; Ma, J.; Yu, X.; Li, Y.; Zhang, L. Silanized MXene/Carbon Nanotube Composites as a Shielding Layer of Polyurethane Coatings for Anticorrosion. *ACS Appl. Nano Mater.* **2022**, *5*, 1408−1418.

(39) Lou, D.; Younes, H.; Yang, J.; Jasthi, B. K.; Hong, G.; Hong, H.; Tolle, C.; Bailey, C.; Widener, C.; Hrabe, R. Enhanced electrical conductivity of anticorrosive coatings by functionalized carbon nanotubes: effect of hydrogen bonding. *Nanotechnology* **2022**, *33*, No. 155704.

(40) Sadiq, M.; Pang, L.; Johnson, M.; Sathish, V.; Zhang, Q.; Wang, D. 2D Nanomaterial, Ti3C2 MXene-Based Sensor to Guide Lung Cancer Therapy and Management. *Biosensors* **2021**, *11*, 40.

(41) Haddadi, S. A.; Hu, S.; Ghaderi, S.; Ghanbari, A.; Ahmadipour, M.; Pung, S. Y.; Li, S.; Feilizadeh, M.; Arjmand, M. Amino-Functionalized MXene Nanosheets Doped with Ce(III) as Potent Nanocontainers toward Self-Healing Epoxy Nanocomposite Coating for Corrosion Protection of Mild Steel. *ACS Appl. Mater. Interfaces* **2021**, *13*, 42074−42093.

(42) Zheng, X.; Tang, J.; Cheng, L.; Yang, H.; Zou, L.; Li, C. Superhydrophobic hollow magnetized Fe3O4 nanospheres/MXene fabrics for electromagnetic interference shielding. *J. Alloys Compd.* **2023**, *934*, No. 167964.

(43) Zheng, X.; Tang, J.; Wang, P.; Wang, Z.; Zou, L.; Li, C. Interfused core-shell heterogeneous graphene/MXene fiber aerogel for high-performance and durable electromagnetic interference shielding. *J. Colloid Interface Sci.* **2022**, *628*, 994−1003.